Kinesin-1 autoinhibition facilitates the initiation of dynein cargo transport

Rongde Qiu, Jun Zhang, and Xin Xiang

Department of Biochemistry and Molecular Biology, The Uniformed Services University of the Health Sciences- F. Edward Hébert School of Medicine, Bethesda, Maryland 20814, USA. Corresponding author email: xin.xiang@usuhs.edu

Abstract

Kinesin-1 undergoes autoinhibition but its functional significance has been unclear. Kinesin-1 transports multiple cargoes including cytoplasmic dynein to the microtubule plus ends. From a genetic screen for *Aspergills* mutants defective in dynein-mediated early endosome transport, we identified a kinesin-1 mutation *kinA*^{K895*} that disrupts kinesin-1 autoinhibition. Consistent with *kinA*^{K895*} making kinesin-1 constitutively active, the mutant proteins accumulate abnormally near the microtubule plus ends. Unexpectedly, our genetic data show that kinesin-1 autoinhibition is unnecessary for transporting its cargoes such as secretory vesicles. Dynein accumulates normally at the microtubule plus ends in the *kinA*^{K895*} mutant. However, the frequency but not the speed of dynein-mediated early endosome transport is significantly decreased, indicating that kinesin-1 autoinhibition facilitates dynein to initiate its cargo transport. Furthermore, kinesin-1 autoinhibition promotes dynein cargo initiation in a way mechanistically distinct from LIS1-promoted dynein switching from its autoinhibited form. Thus, while dynein activation involves dynactin, cargo adapter and LIS1, this study adds kinesin-1 autoinhibition as a new regulatory factor in vivo.

Key words: Kinesin-1 autoinhibition, dynein, phi mutation, cargo adapter, *Aspergillus nidulans*, genetic screen

Introduction

Kinesin-1s are plus-end-directed microtubule motors that transport a variety of cellular cargoes, and defects or dysregulation of kinesin-1s have been implicated in many human diseases (Boecker et al., 2021; Gennerich and Vale, 2009; Hirokawa and Tanaka, 2015; Kelliher et al., 2018; Keren-Kaplan and Bonifacino, 2021; Kruppa and Buss, 2021; Nicolas et al., 2018; Roney et al., 2021). The activity of kinesin-1 is regulated by multiple factors, including its light chains, cargo adapter proteins, an opposite motor that binds to the same cargo, phosphorylation, and microtubule-binding proteins (Ally et al., 2009; Blasius et al., 2007; Byrd et al., 2001; Chen and Sheng, 2013; Coy et al., 1999; Fenton et al., 2021; Ferro et al., 2022; Fu and Holzbaur, 2013; Gindhart et al., 1998; Guardia et al., 2021; Keren-Kaplan and Bonifacino, 2021; Monroy et al., 2020; Sakamoto et al., 2005; Twelvetrees et al., 2019; Verhey and Hammond, 2009; Williams et al., 2014; Xu et al., 2012; Zhao et al., 2021). An important aspect of kinesin-1 regulation is its autoinhibition that involves the interaction between the C-terminal tail and the motor domains (Cai et al., 2007; Coy et al., 1999; Kaan et al., 2011; Verhey and Hammond, 2009; Wong et al., 2009). Recently, an exon27-skipping mutation (Δexon27) in the KIF5A kinesin-1 that causes the devastating neurodegenerative disease Amyotrophic Lateral Sclerosis (ALS) has been linked to a loss of autoinhibition (Baron et al., 2022; Nakano et al., 2022) (Pant et al., 2022, bioRxiv). However, the functional significance of kinesin-1 autoinhibition in normal cells would need to be further dissected.

Cytoplasmic dynein is the minus-end-directed microtubule motor, and defects in dynein and/or its regulator dynactin have been implicated in ALS (Chevalier-Larsen and Holzbaur, 2006; LaMonte et al., 2002; Maimon et al., 2021; Münch et al., 2004). Some vesicular cargos bind both dynein and kinesin-1 via the same cargo adapter (Cox and Spradling, 2006; Fenton et al., 2021; Fu and Holzbaur, 2014)(Canty et al., 2021, bioRxiv; Celestino et al., 2021, bioRxiv), and in this case, loss of kinesin-1 autoinhibition may help overcome the force of dynein to change cargo distribution (Baron et al., 2022; Kelliher et al., 2018). Interestingly, in many cell types including filamentous fungi, mammalian neurons, *C. elegans* neurons, and Drosophila oocytes, dynein itself is a cargo of kinesin-1 (Arimoto et al., 2011; Brendza et al., 2002; Duncan and Warrior, 2002; Egan et al., 2012; Hirokawa et al., 1990; Januschke et al., 2002; Lenz et al., 2006; Twelvetrees et al., 2016; Yamada et al., 2010; Zhang et al., 2003). In mammalian neurons, kinesin-1 interacts with dynein directly and moves dynein towards the microtubule plus ends (Twelvetrees et al., 2016). In filamentous fungi, kinesin-1s are largely (although not completely) responsible for the microtubule plus-end accumulation of dynein and its regulator dynactin (Egan et al., 2012; Han et al., 2001; Lenz et al.,

2006; Penalva et al., 2017; Xiang et al., 2000; Yao et al., 2012; Zhang et al., 2003; Zhang et al., 2010). This accumulation is important for the retrograde transport of dynein cargoes such as early endosomes, most likely because it enhances the chance for dynein-cargo interaction (Abenza et al., 2009; Egan et al., 2012; Lenz et al., 2006; Zekert and Fischer, 2009; Zhang et al., 2010). It is important to note that the plus-end-directed transport of early endosomes does not use kinesin-1 but uses kinesin-3 (Lenz et al., 2006; Wedlich-Soldner et al., 2002; Zekert and Fischer, 2009). Dynein transports early endosomes away from the plus ends with the help of dynactin and the FTS-Hook-FHIP complex (Bielska et al., 2014; Yao et al., 2014; Zhang et al., 2014; Zhang et al., 2011b). The mechanism of dynein-mediated early endosome transport is conserved and has been further dissected using mammalian proteins (Christensen et al., 2021; Guo et al., 2016; Lau et al., 2021; Olenick et al., 2019; Yeh et al., 2012), but factors regulating this process need to be further studied. In the case of kinesin-1, it was unknown whether its autoinhibition plays a role in the initiation of dynein cargo transport from the microtubule plus ends. During a forward genetic screen for mutants defective in dynein-mediated early-endosome transport in *Aspergillus nidulans*, we serendipitously identified a nonsense mutation *kinA*^{K895*} causing a loss of kinesin-1 autoinhibition. Our analyses suggest that this autoinhibition is unnecessary for kinesin-1 to transport its own cargos including dynein and secretory vesicles, but it is important for the initiation of dynein-mediated early endosome transport.

Results and Discussion:

Identifying *kinA*^{K895*} as a causal mutation affecting dynein-mediated early endosome transport.

In *A. nidulans*, the plus ends of microtubules face the hyphal tip and minus ends are either at the spindle-pole body or at septum (Efimov et al., 2006; Egan et al., 2012; Gao et al., 2019; Han et al., 2001; Konzack et al., 2005; Oakley et al., 1990; Xiong and Oakley, 2009; Zeng et al., 2014; Zhang et al., 2017b). Dynein normally accumulates at the microtubule plus ends near the hyphal tip, as represented by the comet-like structures (Han et al., 2001; Xiang et al., 2000). A defect in dynein-mediated early endosome transport causes an abnormal accumulation of early endosomes and their hitchhiking cargoes near the hyphal tip (Abenza et al., 2009; Egan et al., 2012; Lenz et al., 2006; Salogiannis and Reck-Peterson, 2017; Zekert and Fischer, 2009; Zhang et al., 2011b; Zhang et al., 2010). To find additional dynein regulators, we performed genetic screens for early-endosome distribution (*eed*) mutants, which have allowed us to find novel dynein regulators (Xiang and Qiu, 2020). In this study, we performed UV mutagenesis using a strain containing mCherry-labeled RabA and GFP-labeled dynein heavy chain, which allows observation of early endosomes and dynein respectively (Pinar and Peñalva, 2021; Zhuang et al., 2007). The *eedE*16 mutant isolated after UV mutagenesis formed a colony smaller than that of a wild-type strain (Figure 1A). In the mutant, GFP-dynein formed the plus-end comets (Figure 1B), but early endosomes abnormally accumulated near the hyphal tip (Figure 1B).

To identify the *eedE*16 mutation, we took a whole-genome sequencing approach as described previously (Qiu et al., 2020). Whole-genome sequencing was done using the genome sequencing and bioinformatic service of Genewiz (www.genewiz.com). We used the software Integrative Genomics Viewer (IGV 2.4.3) to visualize the genomic sequencing data to identify the mutation. The *eedE16* mutation was found in *kinA*, which encodes the only kinesin-1 in *A. nidulans*, with 927 amino acids (Requena et al., 2001). The mutation substituted an A with T that changed the codon for lysine (K) (AAG) to a stop codon (TAG) at residue 895. This results in the deletion of 33 amino acids at the C-terminus of KinA. The C-terminus of Drosophila Kinesin-1 or a human kinesin-1 KIF5A contains two important regions: the IAK motif involved in autoinhibition (Kaan et al., 2011), and the RKRYQ region responsible for ATP-independent microtubule binding (Lu et al., 2016; Winding et al., 2016). The IAK motif involved in autoinhibition is conserved in KinA but the residues for ATP-independent microtubule binding are not (Supplemental Figure 1). Importantly, K895 corresponds to K within the IAK motif (Figure 1C; Supplemental Figure 1), and the mutation should delete it and the rest of the C-terminus. Thus, the *kinA*^{K895*} mutation is predicted to eliminate kinesin-1 autoinhibition.

KinA$^{(1-894)}$-GFP forms an abnormally strong accumulation near the microtubule plus ends.

To compare the behaviors of the wild-type and the *kinA*^{K895*} mutant kinesin-1s, we constructed strains

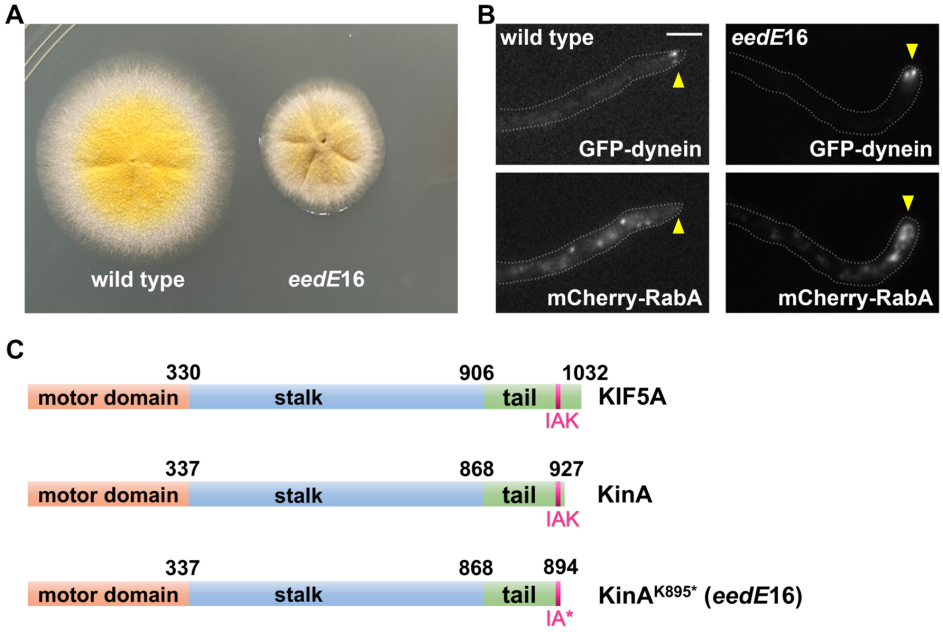

Figure 1. Phenotype of the *eedE*16 mutant and position of the causal mutation in kinesin-1. (A) Colony phenotypes of the *eedE*16 mutant and a wild-type strain. (B) Microscopic images showing the distributions of GFP-dynein and mCherry-RabA-labeled early endosomes (mCherry-RabA) in wild type and the mutant. Bar, 5 μm. Although bi-directional movements of mCherry-RabA-labeled early endosomes are not completely abolished, most of the *eedE*16 hyphal tips (~80%) show an obvious accumulation of mCherry-RabA signals (n=130). Hyphal tip is indicated by a yellow arrowhead. (C) Domain structures of kinesin-1 proteins in human (KIF5A) and *A. nidulans* (KinA). Positions of the IAK motif involved in kinesin-1 autoinhibition and the *eed*E16 mutation *kinA*^{K895*} within the IAK motif are indicated.

with either the *kinA*-GFP or the *kinA*$^{(1-894)}$-GFP fusion gene integrated at the endogenous *kinA* locus (Figure 2A). KinA-GFP formed a diffuse background in the cytoplasm with only very faint plus-end comet-like structures near the hyphal tip (Figure 2B). In contrast, KinA$^{(1-894)}$-GFP signals were strongly accumulated at the hyphal tip near microtubule plus ends. This is consistent with the localization pattern of uninhibited kinesin-1s in neurons and also in another fungus *Neurospora crassa* (Baron et al., 2022; Seiler et al., 2000; Twelvetrees et al., 2016). As expected, early endosomes (labeled with mCherry-RabA) distributed normally in the kinA-GFP strain but accumulated abnormally near the hyphal tip in the kinA$^{(1-894)}$-GFP strain just like in the *kinA*^{K895*} mutant (Figure 2B). Using strains containing the conditional-null allele of dynactin Arp1 (*alcA-nudK*^{Arp1}) or dynein heavy chain (*alcA-nudA*^{HC}), we further showed that the prominent hyphal-tip accumulation of KinA$^{(1-894)}$-GFP signals occurs in the absence of dynein or dynactin (Figure 2C).

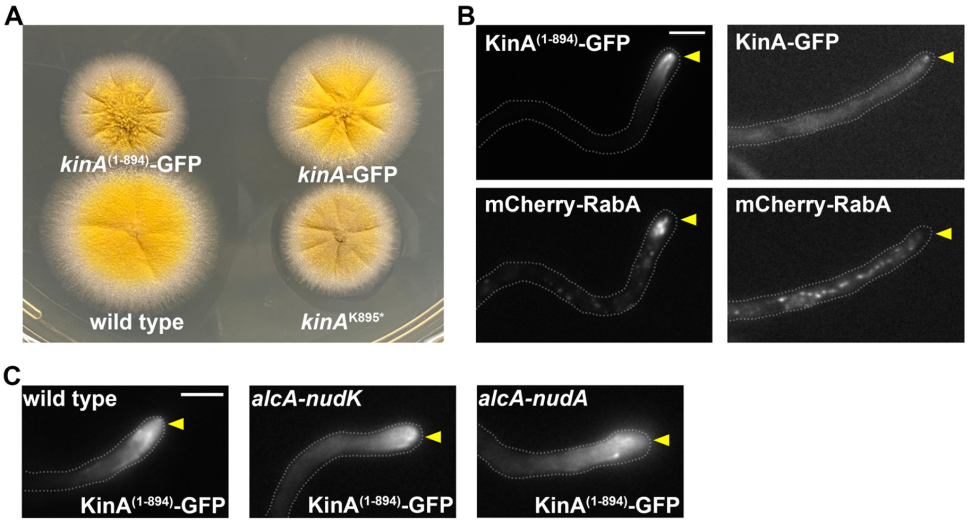

Figure 2. KinA$^{(1-894)}$-GFP fusion proteins form a prominent accumulation near the microtubule plus ends. (A) Colony phenotypes of the strains containing *kinA*-GFP and *kinA*$^{(1-894)}$-GFP in comparison to wild type and the *eed*E16 mutant *kinA*^{K895*}. (B) Localization of KinA-GFP or KinA$^{(1-894)}$-GFP and mCherry-RabA-labeled early endosomes in strains containing one of the GFP fusions. Most (~87.5%) of the hyphal tips of the *kinA*$^{(1-894)}$-GFP mutant show an abnormal accumulation of early endosomes (n=32). Hyphal tip is indicated by a yellow arrowhead. Bar, 5 μm. (C) The hyphal-tip localization of KinA$^{(1-894)}$-GFP is independent of dynein or dynactin. Images were taken from cells grown on glucose, a repressive medium for the regulatable *alcA* promoter. The *alcA-nudK*^{Arp1} or the *alcA-nudA*^{HC} conditional-null allele allows the expression of dynactin Arp1 or dynein heavy chain to be shut off on glucose. Hyphal tip is indicated by a yellow arrowhead. Bar, 5 μm.

Kinesin-1 autoinhibition is not critical for the transport of its own cargo.

We next sought to determine if kinesin-1 auto-inhibition is critical for its cargo-transporting function. To do that, we compared the effect caused by the C-terminal truncated *kinA* with that of the previously constructed Δ*kinA* allele (Requena et al., 2001). The colony formed by the *kinA*^{K895*} mutant is bigger than the Δ*kinA* mutant (Figure 3A, 3B), suggesting that function of kinesin-1 is partially retained in the uninhibited mutant. In filamentous fungi, both kinesin-1 and myosin-V are capable of transporting secretory vesicles to support hyphal tip extension (Pantazopoulou et al., 2014; Penalva et al., 2017; Schuchardt et al., 2005; Schuster et al., 2012). In *A. nidulans*, the Δ*kinA* or the *alcA-myoV* (myosin-V conditional-null mutant) single mutant forms a colony whose size is smaller than that of wild type, but the Δ*kinA*, *alcA*-myoV double mutant is nearly inviable when grown on glucose that shuts off the expression of myosin-V (Zhang et al., 2011a) (Figure 3C). In contrast, the colony of the *kinA*$^{(1-894)}$-GFP, *alcA-myoV* double mutant was slightly bigger than the *alcA-myoV* single mutant (Figure 3C, 3D). To confirm this result, we also made a *kinA*$^{(1-894)}$-GFP, Δ*myoV* double mutant. The Δ*myoV* single mutant formed a compact colony (Taheri-Talesh et al., 2012). In striking contrast to the nearly lethal phenotype of the Δ*kinA*, Δ*myoV* double mutant (Penalva et al., 2017), the *kinA*$^{(1-894)}$-GFP, Δ*myoV* double mutant formed a colony whose diameter is similar to that of the Δ*myoV* single mutant (Figure 3C, 3D). These genetic data strongly indicate that auto-inhibition is not necessary for the general transporting function of kinesin-1 involved in supporting hyphal growth. Consistent with this conclusion, Rab11-marked secretory vesicles, which are cargoes of kinesin-1 and myosin-V (Pantazopoulou et al., 2014; Penalva et al., 2017) (Pinar et al., 2021 bioRxiv), reach the hyphal tip in the *kinA*^{K895*}, Δ*myoV* double mutant just like in the Δ*myoV* single mutant (Figure 3E).

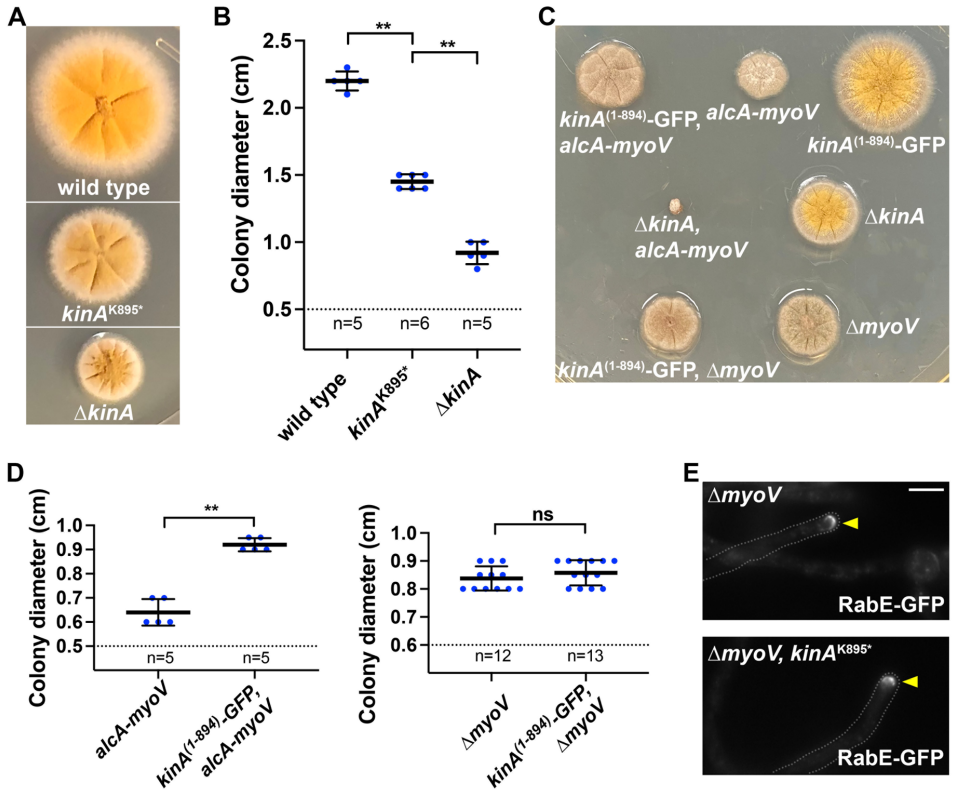

Figure 3. Kinesin-1 autoinhibition is not critical for its own cargo transport function. (A) Colony phenotypes of a wild-type strain, the *kinA*^{K895*} mutant and the Δ*kinA* mutant. (B) A quantitative analysis of colony diameter of the wild-type strain, the *kinA*^{K895*} mutant and the Δ*kinA* mutant. Scatter plots with mean and S.D. values were generated by Prism 9. The Mann-Whitney test (unpaired, two tailed) was used for analyzing two data sets at a time without assuming normal distribution of the data. **p<0.01. (C) Colony phenotypes of the single and double myosin-V (*myoV*) and kinesin-1 (*kinA*) mutants. (D) A quantitative analyses of colony diameters of *alcA-myoV* and *kinA*$^{(1-894)}$-GFP, *alcA-myoV* (**p<0.01; unpaired, Mann-Whitney test) and of Δ*myoV* and *kinA*$^{(1-894)}$-GFP, Δ*myoV*. The difference between the Δ*myoV* and *kinA*$^{(1-894)}$-GFP, Δ*myoV* strains is not significant (ns) at p=0.05 (unpaired, Mann-Whitney test). (E) Microscopic images showing the hyphal-tip signals of RabE-GFP in Δ*myoV* and the Δ*myoV*, *kinA*^{K895*} double mutant. Hyphal tip is indicated by a yellow arrowhead. Bar, 5 μm.

Loss of kinesin-1 autoinhibition affects the initiation of dynein-mediated early endosome transport

We next quantitated the microtubule plus-end dynein localization in the *kinA*^{K895*} mutant, and we did this in the Δ*hookA* background missing the cargo adapter (Note that cargo adapters would activate dynein to leave the plus ends (Baumbach et al.,

2017; Jha et al., 2017; Lammers and Markus, 2015; McKenney et al., 2014; Qiu et al., 2019; Schlager et al., 2014; Splinter et al., 2012)). In the *kinA*^{K895*}, Δ*hookA* double mutant, the plus-end dynein comet intensity is similar to that in the Δ*hookA* single mutant (Figure 4A, 4B). This is consistent with a previous study showing that the posterior localization of dynein during Drosophila oogenesis needs kinesin-1 but not its IAK region implicated in autoinhibition (Williams et al., 2014). Thus, although uninhibited KinA tends to move to the microtubule plus ends without carrying its cargo, it can still carry dynein to the plus end. This may be explained by in vitro data showing that an uninhibited kinesin-1 is much more likely to land on a microtubule or have a higher processivity than a normally autoinhibited kinesin-1 (Baron et al., 2022) (Pant et al., 2022 bioRxiv).

To better understand the effect of kinesin-1 autoinhibition on dynein function, we measured the frequency and speed of dynein-mediated early endosome movement in *kinA*^{K895*} mutant in comparison to the wild-type control. We found that the frequency but not the speed is significantly reduced in the mutant (Figure 4C, 4D, 4E). Thus, although dynein can be targeted to the microtubule plus ends in the *kinA*^{K895*} mutant, its function in initiating cargo transport is compromised. This defect is conceptually similar to (although less severe than) that caused by loss of LIS1, a dynein regulator required for the initiation of dynein-mediated early endosome transport in filamentous fungi (Egan et al., 2012; Lenz et al., 2006)

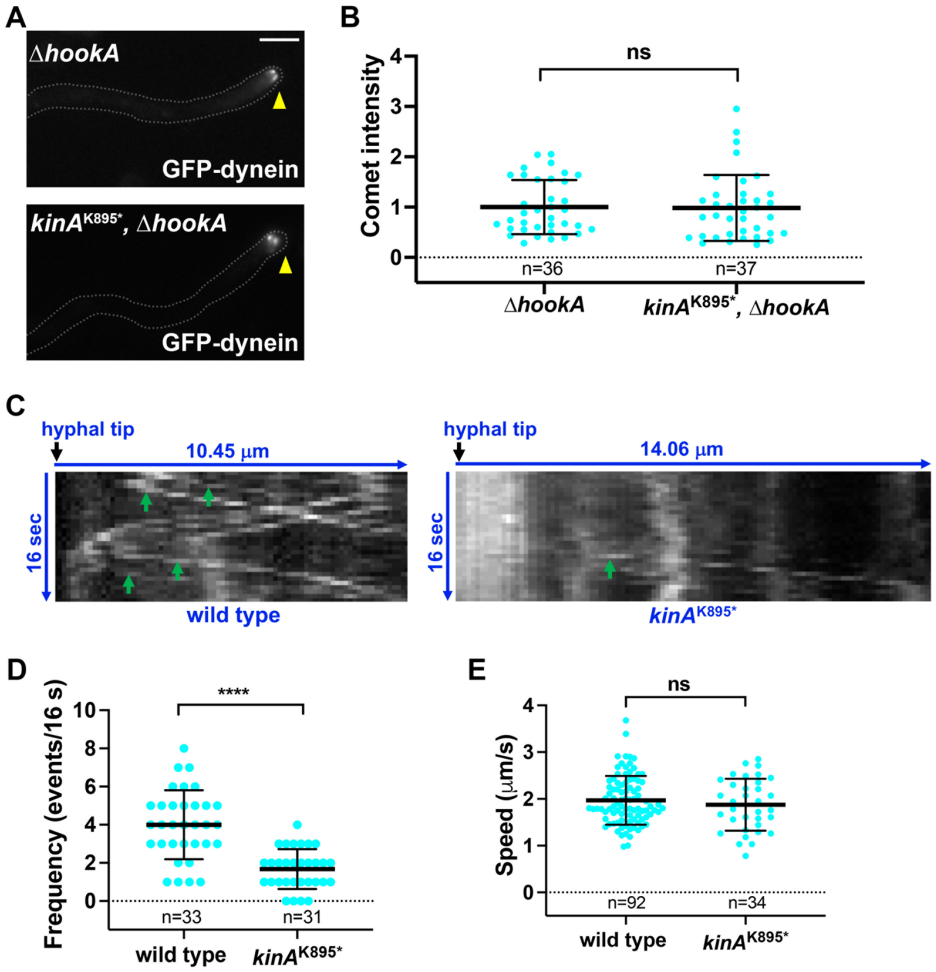

Figure 4. Loss of kinesin-1 autoinhibition does not affect dynein accumulation at the microtubule plus ends but affects the initiation of dynein-mediated early endosome transport. (A) Microscopic images showing the hyphal tip signals of GFP-dynein in the Δ*hookA* single and the *kinA*^{K895*}, Δ*hookA* double mutant. Hyphal tip is indicated by a yellow arrowhead. Bar, 5 μm. (B) A quantitative analysis on GFP-dynein comet intensity in Δ*hookA* and the Δ*hookA*, *kinA*^{K895*} double mutant. All values are relative to the average value for Δ*hookA*, which is set as 1. Scatter plots with mean and S.D. values were generated by Prism 9. The Mann-Whitney test (unpaired, two tailed) was used for analyzing the two data sets without assuming normal distribution of the data. (C) Kymographs showing the movements of early endosomes in wild type and the *kinA*^{K895*} mutant. Green arrows indicate dynein-mediated movements away from the hyphal tip. (D) A quantitative analysis on the frequency of dynein-mediated transport in wild type (n=33 hyphal tips) and the *kinA*^{K895*} mutant (n=31 hyphal tips). Scatter plots with mean and SD values were generated by Prism 9. ****p<0.0001 (unpaired, Mann-Whitney test, Prism 9). (E) A quantitative analysis on the speed of dynein-mediated early endosome movement in wild type (n=92 movements) and the *kinA*^{K895*} mutant (n=34 movements). The difference between wild type and the mutant is not significant (ns) at p=0.05 (unpaired, Mann-Whitney test, Prism 9).

The role of kinesin-1 autoinhibition in dynein cargo initiation differs from that of LIS1

Dynein activation involves conformational changes of the dynein heavy chain dimer from an auto-inhibited "phi" conformation to the open conformation (Torisawa et al., 2014; Zhang et al., 2017a), and binding of dynactin and cargo adapter to the dynein tail causes dynein to assume a parallel conformation allowing it to move processively (Zhang et al., 2017a). The phi mutation keeps dynein open, thereby facilitating its activation (Zhang et al., 2017a). In *A. nidulans*, either the phi mutation (*nudA*^{R1602,K1645E}) or overexpression of the ΔC-HookA adapter causes a dramatic dynein relocation from the microtubule plus ends to the minus ends on septa (Qiu et al., 2019). Upon loss of LIS1 function in the *nudF* mutants, overexpression of ΔC-HookA fails to drive this relocation but the phi mutation is able to do so, suggesting that a main function of NudF/LIS1 is to overcome the autoinhibited phi conformation (Qiu et al., 2019). This notion is consistent with data from budding yeast or in vitro (Elshenawy et al., 2020; Gillies et al., 2022; Htet et al., 2020; Marzo et al., 2020; Qiu et al., 2019). In the *kinA*^{K895*} mutant, either the phi mutation or overexpression of the ΔC-HookA adapter can still cause dynein relocation to the minus ends on septa like in cells containing the wild-type *kinA* allele, but in either case the relocation is partially defective as evidenced by the more easily observable plus-end dynein comets and the reduced septal signals (Figure 5A, 5B, 5C, 5D). Importantly, quantitation of septal dynein signals indicates that overexpression of the ΔC-HookA adapter is more effective than the phi mutation in driving dynein relocation in the *kinA*^{K895*} mutant (Figure 5B, 5C, 5D), which is opposite to the situation in the *nudF* (lis1) mutants. Furthermore, the phi mutation significantly reduces the hyphal-tip early endosome accumulation in the *nudF*6 mutant but not in the *kinA*^{K895*} mutant (Figure 5E, 5F). Thus, kinesin-1 autoinhibition is involved in the initiation of dynein cargo transport with a mechanism different from that of LIS1-mediated dynein opening.

How kinesin-1 autoinhibition facilitates the initiation of dynein cargo transport remains an important question. Kinesin-mediated transport of dynein to the microtubule plus ends has been reported from fungi to mammalian neurons (although kinesin-7 instead of kinesin-1 is used in budding yeast) (Arimoto et al., 2011; Brendza et al., 2002; Carvalho et al., 2004; Duncan and Warrior, 2002; Egan et al., 2012; Hirokawa et al., 1990; Januschke et al., 2002; Lenz et al., 2006; Roberts et al., 2014; Twelvetrees et al., 2016; Yamada et al., 2010; Zhang et al., 2003). In several systems, the plus-end accumulation of dynein and its regulator dynactin play an important role in cargo binding or the initiation of cargo transport (Lenz et al., 2006; Lloyd et al., 2012; Markus and Lee, 2011; Moughamian and Holzbaur, 2012; Splinter et al., 2012; Vaughan et al., 2002). However, it is not known how kinesin-1 regulation plays a role in preparing dynein-dynactin for cargo binding and transport from the microtubule plus end. From our current data, we speculate that kinesin-1 autoinhibition can happen after LIS1-mediated dynein opening but needs to occur either before or after dynein-cargo interaction to facilitates the interaction and/or cargo-adapter-mediated dynein activation. If kinesin-1 fails to undergo autoinhibition, even if dynein is switched to the open conformation, it will still fail to initiate cargo transport. Thus, kinesin-1 autoinhibition should be considered as a factor that cooperates with LIS1, dynactin and cargo adapter to initiate dynein cargo transport in cells where kinesin-1-mediated dynein accumulation at the microtubule plus ends is important for dynein cargo transport.

Recently, multiple studies indicate that an ALS-causing mutation (Δexon27) that changes the C-terminus of KIF5A is a gain-of-function mutation that leads to a loss of autoinhibition (Baron et al., 2022; Nakano et al., 2022) (Pant et al., 2022 bioRxiv). Since the mutation creates a new C-terminus, it needs to be further addressed whether it is the loss of autoinhibition *per se* or the creation of a new C-terminus that leads to ALS. Our analysis on *A. nidulans* diploids has shown that the *kinA*^{K895*} or the *kinA*$^{(1-894)}$-GFP allele is also a gain-of-function mutation that partially affects dynein-mediated early endosome transport in the presence of a wild-type copy of *kinA* (Supplemental Figure 2). As dynein defects have been linked to ALS (Chevalier-Larsen and Holzbaur, 2006; Gershoni-Emek et al., 2016; Hafezparast et al., 2003; Ikenaka et al., 2013; Kieran et al., 2005; LaMonte et al., 2002; Maimon et al., 2021; Mentis et al., 2022; Münch et al., 2004; Stavoe and Holzbaur, 2019; Ström et al., 2008), it is likely that a partial defect in dynein function contributes to ALS caused by the gain-of-function mutations in KIF5A. Future studies will be needed to test this idea.

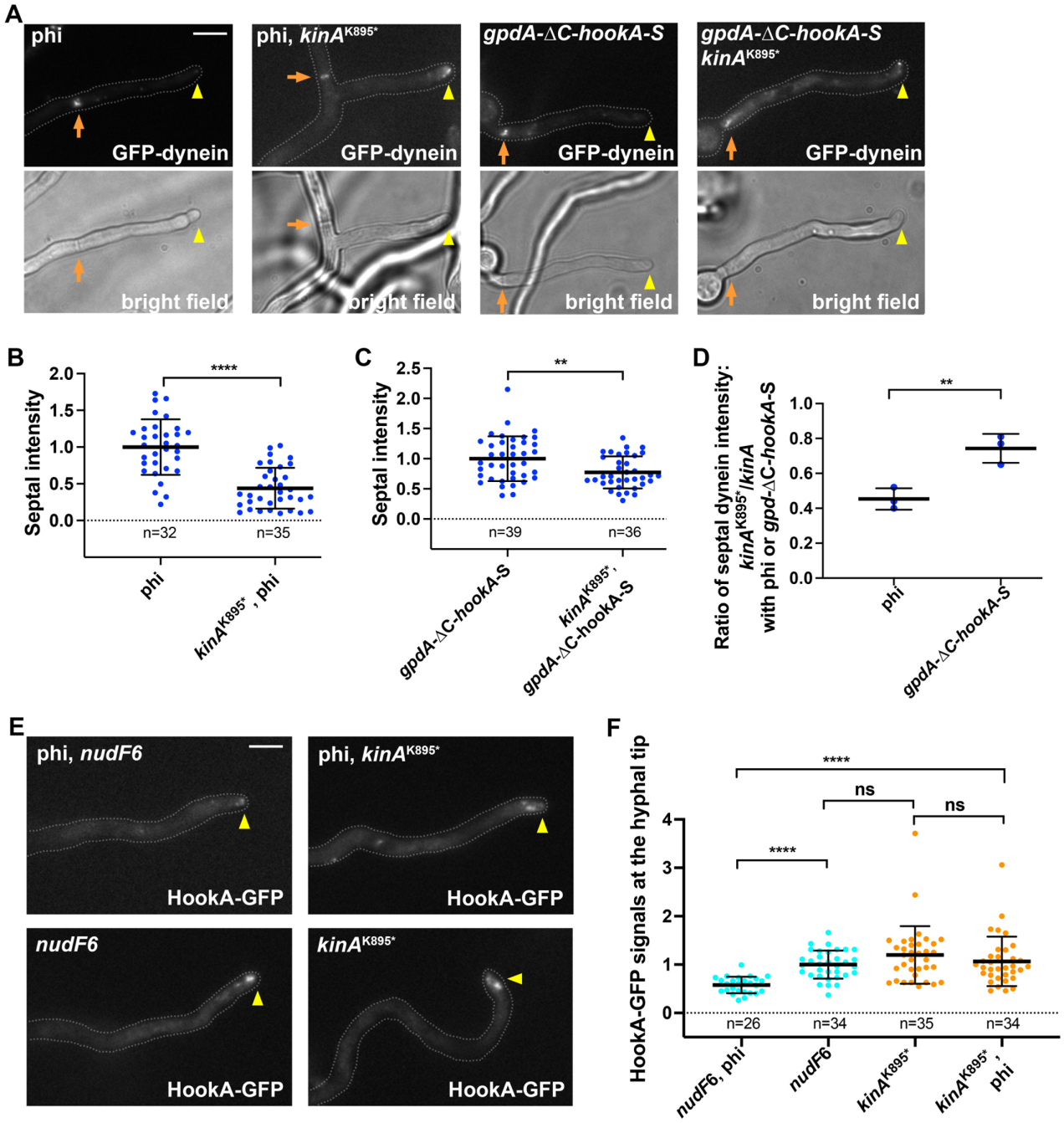

Figure 5. Effects of factors involved in dynein activation on the *kinA*^{K895*} mutant. (A) Dynein localization in the phi single mutant and the phi, *kinA*^{K895*} double mutant, and that upon overexpression of the cargo adapter ΔC-HookA in the wild-type background (*gpdA*-ΔC-*hookA*-S) and in the *kinA*^{K895*} background (*kinA*^{K895*}, *gpdA*-ΔC-*hookA*-S). Bright-field images are shown below to indicate hyphal shape and position of septum. Hyphal tip is indicated by a yellow arrowhead and septum by a brown arrow. Bar, 5 μm. (B) Quantitation of dynein signals at septa (for the two phi-mutation-containing strains). All values are relative to the average value for the phi single mutant, which is set as 1. Scatter plots with mean and SD values were generated by Prism 9. ****p<0.0001 (unpaired, Mann-Whitney test, Prism 8). (C) Quantitation of dynein signals at septa (for the two *gpdA*-ΔC-*hookA*-S-containing strains). All values are relative to the average value for the *gpdA*-ΔC-*hookA*-S strain, which is set as 1. Scatter plots with mean and SD values were generated by Prism 9. **p<0.01 (unpaired, Mann-Whitney test, Prism 9). (D). Ratio of the *kinA*^{K895*} mutant value to the wild type value in the phi or the *gpdA*-ΔC-*hookA*-S strains. Data were from three experiments. Scatter plots with mean and SD values were generated by Prism 9. **p<0.01 (unpaired, Mann-Whitney test, Prism 9). (E) Effect of the phi mutation on the hyphal-tip accumulation of early endosomes (labeled by HookA-GFP) in the *nudF*6 (*lis1*) and *kinA*^{k895*} mutants. Images of HookA-GFP in the *nudF*6 single and the *nudF*6, phi double mutant, and in the *kinA*^{k895*} single and the *kinA*^{k895*}, phi double mutant. Because we routinely culture the *kinA*^{k895*} mutant at 32°C, we used 32°C for culturing the *nudF*6 mutant in this experiment. Note that although the function of NudF/LIS1 is not completely lost at 32°C (a semi-restrictive temperature), the hyphal-tip accumulation of HookA-GFP signals is very obvious in the single *nudF*6 mutant. Bar, 5 μm. (F) A quantitative analysis on hyphal-tip accumulated HookA-GFP signals. The average value for the *nudF*6 strain is set as 1. Scatter plots with mean and S.D. values were generated by Prism 9. ****p<0.0001; ns, non-significant or p>0.05 (Kruskal-Wallis with Dunn's multiple comparisons test, unpaired).

Materials and Methods

A. nidulans strains and media

A. nidulans strains used in this study are listed in Supplemental Table 1. UV mutagenesis on spores of *A. nidulans* strains was done as previously described (Willins et al., 1995; Xiang et al., 1999). Solid rich medium was made of either YAG (0.5% yeast extract and 2% glucose with 2% agar) or YAG+UU (YAG plus 0.12% uridine and 0.12% uracil). Genetic crosses and diploid construction were done by standard methods. Solid minimal medium containing 1% glucose was used for selecting progeny from a cross and for selecting diploids. For live cells imaging experiments, cells were cultured in liquid minimal medium containing 1% glycerol for overnight at 32°C. All the biochemical analyses (for confirming strain genotypes) and genomic DNA preparation were done using cells grown at 32°C for overnight in liquid YG rich medium (0.5% yeast extract and 2% glucose). For a few experiments using strains containing the *alcA-nudK*^{Arp1} or *alcA-nudA*^{HC} allele, we harvested spores from the solid minimal medium containing 1% glycerol and cultured them in liquid minimal medium containing 1% glucose for imaging analysis.

Construction of the strain containing the *kinA*-GFP allele at the *kinA* locus

Strains were constructed by using standard procedures used in *A. nidulans* (Nayak et al., 2006; Szewczyk et al., 2006; Yang et al., 2004). For constructing the *kinA*-GFP fusion, we used the following six oligos to amplify genomic DNA from RQ177 (Qiu et al., 2018) that contains the GFP-*AfpyrG* fusion (Yang et al., 2004): K5U (AGTCTTTCAGAGACGCAGGG), BW2 (TCGTC TATCAAAAAACCAACTTGTG), KF3 (CACAAGTTGGTTTTTT GATAGACGAGGAGCTGGTGCAGGCG), BW4 (CCATCTAG ATATCTGCAGGAAGGGGCTGTCTGAGAGGAGGCACTG), BW5 (CCCCTTCCTGCAGATATCTAGATGG) and BW6 (GCTGAAGTTGGTTGATTTGCGG). Specifically, K5U and BW2 were used to amplify the ~1-kb fragment in the coding region, and BW5 and BW6 were used to amplify the ~1-kb fragment in the 3' untranslated region, and KF3 and BW4 were used to amplify the ~2.7-kb GFP-*AfpyrG* fragment using genomic DNA from the RQ177 strain (Qiu et al., 2018). We then used two oligos, K5U and BW6, for a fusion PCR of the three fragments to generate the ~4.6-kb *kinA*-GFP-AfpyrG fragment that we used to transform into XY42 containing Δ*nkuA* (Nayak et al., 2006) and mCherry-RabA (Abenza et al., 2009; Qiu et al., 2018; Zhang et al., 2010). The transformants were screened by microscopically observing the GFP signals, and the presence of the *kinA*-GFP fusion was confirmed by western blotting analysis with a polyclonal anti-GFP antibody from Clontech. In addition, we also performed a diagnostic PCR to verify the correct integration using oligos K5UTR (GAACGACCTCACAGACTCA) and AFpyrG3 (GTTGCCAGG TGAGGGTATTT).

Construction of the strain containing the *kinA*$^{(1-894)}$-GFP allele at the *kinA* locus

For constructing the *kinA*$^{(1-894)}$-GFP strain, we made the *kinA*$^{(1-894)}$-GFP-*AfpyrG* fragment by inserting the GFP-*AfpyrG* fragment into the *kinA*^{K895*} mutation site right before the stop codon. The following four oligos were used to make the *kinA*$^{(1-894)}$-GFP-*AfpyrG* construct: K5U, K895.R (GCACCAGCTCCA GCGATTCGGGAGCCAG), K895.F (AATCGCTGGAGCTGGT GCAGGCG) and BW6. Specifically, K5U and K895.R were used to amplify a ~0.9-kb fragment of the 5' coding region, and K895.F and BW6 were used to amplify the ~2.7-kb GFP-*AfpyrG* fragment using genomic DNA from the RQ197 strain (containing *kinA*-GFP) as template. We then used two oligos, K5U and BW6, for a fusion PCR to fuse the two fragments to generate the ~4.5-kb *kinA*$^{(1-894)}$-GFP-*AfpyrG* fragment that we used to transform the XY42 strain and the RQ54 strain. The transformants were screened by microscopically observing the GFP signals and further confirmed by a western blotting analysis with a polyclonal anti-GFP antibody from Clontech. In addition, we also performed a diagnostic PCR to verify the correct integration using oligos K5UTR (GAACGACCTCACAGACTCA) and GFP-5R (CAGTGAAAAGTTCTTCTCCTTTACT).

Live-cell imaging and analyses

All images were captured using an Olympus IX73 inverted fluorescence microscope linked to a PCO/Cooke Corporation Sensicam QE cooled CCD camera. An UPlanSApo 100x objective lens (oil) with a 1.40 numerical aperture was used. A filter wheel system with GFP/mCherry-ET Sputtered series with high transmission (Biovision Technologies) was used. For all images, cells were grown in the LabTek Chambered #1.0 borosilicate coverglass system (Nalge Nunc International, Rochester, NY). The IPLab software was used for image acquisition and analysis. Image labeling was done using Microsoft PowerPoint and/or Adobe Photoshop. For quantitation of dynein signal intensity, a region of interest (ROI) was selected and the Max/Min tool of the IPLab program was used to measure the maximal intensity within the ROI. The ROI box was then dragged to a nearby area outside of the cell to take the background value, which was then subtracted from the intensity value. For quantitation of HookA-GFP-marked early endosome accumulation at the hyphal tip, the total signals at the hyphal tip (Sum) was measured, and background subtracted the same way. Hyphae were chosen randomly from images acquired under the same experimental conditions. For measuring the signal intensity of a MT plus-end comet formed by GFP-dynein, only the comet close to hyphal tip was measured. For measuring GFP-dynein signal intensity at septa, usually only the septum most proximal to the hyphal tip was measured. Images were taken at room temperature immediately after the cells were taken out of the incubators. Cells were cultured overnight in minimal medium with 1% glycerol and supplements at 32°C.

Statistical analysis

All statistical analyses were done using GraphPad Prism 9 for macOS (version 9.2.0, 2021). The D'Agostino & Pearson normality test was performed on all data sets. For all data sets, non-parametric tests were used without assuming Gaussian distribution, except that Ordinary one-way ANOVa was used for the analysis presented in Supplemental Figure 2B. Specifically, the Kruskal-Wallis ANOVA test (unpaired) with Dunn's multiple comparisons test was used for analyzing multiple data sets, and the Mann-Whitney test (unpaired, two tailed) was used for analyzing two data sets. Note that adjusted p values were generated from the Kruskal-Wallis ANOVA test with Dunn's multiple comparisons test. In all figures, **** indicates $p<0.0001$, *** indicates $p<0.001$, ** indicates $p<0.01$, * indicates $p<0.05$ *, and "ns" indicates $p>0.05$.

Acknowledgements

We thank Berl Oakley, Elizabeth Oakley, Miguel Peñalva and Reinhard Fischer for Aspergillus strains. This work was funded by the National Institutes of Health RO1 GM121850 (to X. Xiang) and R35 GM140792 (to X. Xiang). Disclaimer: The opinions and

assertions expressed herein are those of the author(s) and do not necessarily reflect the official policy or position of the Uniformed Services University or the Department of Defense.

Author contributions

R.Q. and X.X. conceived the experiments. R.Q., J.Z. and X.X. carried out the experiments. X.X. and R.Q. wrote the manuscript, which was read and edited by all authors.

Declaration of interests

The authors declare no competing interest.

Supplemental Materials (1 supplemental table and 2 supplemental figures):

Supplemental Table 1. *Aspergillus nidulans* strains used in this study

Strain	Genotype	Source
alcA-myoV	*alcA*-GFP-*myoV-pyr4*; *pyrG*89; *pyroA*4; *wA*3	(Zhang et al., 2011a)
JZ504	GFP-*nudA*^{HC}; Δ*hookA-AfpyrG; argB2::[argB*-alcAp*::mCherry-*RabA]*; *pyroA*4	(Qiu et al., 2021)
LO1830	Δ*myoV*::*AfpyrG; pyrG*89; *pyroA*4; *riboB*2; Δ*nkuA::argB* (Note: *myoV* was called *myoE* in the original publication)	(Taheri-Talesh et al., 2012)
RQ2	GFP-*nudA*^{HC}*; argB2::[argB*-alcAp*::mCherry-*RabA];* Δ*nkuA::argB; pyrG*89; *pyroA*4; *yA*2	(Qiu et al., 2013)
RQ54	*argB2::[argB*-alcAp*::mCherry-*RabA];* Δ*nkuA::argB; pyrG*89; *pyroA*4; *wA*2	(Qiu et al., 2013)
RQ102	GFP-*nudA*^{HC}; Δ*hookA-AfpyrG; argB2::[argB*-alcAp*::mCherry-*RabA]*; *pantoB100*; *yA2*	(Qiu et al., 2021)
RQ287	GFP-*nudA*^{HC}; *gpdA*-ΔC-*hookA*-S-*AfpyrG; yA*2	(Qiu et al., 2019)
RQ294	GFP-*nudA*^{R1602,K1645E}; *argB2::[argB*-alcAp*::mCherry-*RabA]*; Δ*nkuA::argB*; *pyroA*4; *yA*2	(Qiu et al., 2019)
XX213	Δ*kinA-pyr*4; GFP-*nudA*^{HC}*; argB2::[argB*-alcAp*::mCherry-*RabA]*	(Zhang et al., 2010)
XX222	GFP-*nudA*^{HC}*; argB2::[argB*-alcAp*::mCherry-*RabA]*; *yA2*; *pantoB*100	(Zhang et al., 2010)
XY42	*argB2::[argB*-alcAp*::mCherry-*RabA]*; Δ*nkuA::argB*; *pyrG*89; *yA2*; *pantoB*100	(Qiu et al., 2018)
Mu16 or *eedE*16	*kinA*^{K895*}; GFP-*nudA*^{HC}*; argB2::[argB*-alcAp*::mCherry-*RabA]*; *yA2*; *pantoB*100	This work
RQ197	*kinA*-GFP-*AfpyrG*; *argB2::[argB*-alcAp*::mCherry-*RabA]*; Δ*nkuA::argB*; *pyrG*89; *yA2*; *pantoB*100	This work
RQ358	*kinA*$^{(1-894)}$-GFP-*AfpyrG*; *argB2::[argB*-alcAp*::mCherry-*RabA]*; Δ*nkuA::argB*; *pyrG*89; *yA2*; *pantoB*100	This work
RQ360	*kinA*$^{(1-894)}$-GFP-*AfpyrG*; *alcA-nudK*^{Arp1}*-pyr4*; possibly p25-S-tag-A*fpyrG*; possibly Δ*nkuA::argB*; possibly *pyrG*89	This work
RQ361	*kinA*$^{(1-894)}$-GFP-*AfpyrG*; *alcA-nudA*^{HC}*-pyr4*; *argB2::[argB*-alcAp*::mCherry-*RabA]*; possibly Δ*nkuA::argB*; possibly *pyrG*89	This work
RQ362	*kinA*$^{(1-894)}$-GFP-*AfpyrG*; Δ*hookA-AfpyrG; argB2::[argB*-alcAp*::mCherry-*RabA]*; Δ*nkuA::argB*; possibly *pyrG*89	This work
RQ366	*kinA*-GFP-*AfpyrG*; Δ*hookA-AfpyrG; argB2::[argB*-alcAp*::mCherry-*RabA]*; Δ*nkuA::argB*; possibly *pyrG*89	This work
XX679	*kinA*^{K895*}; GFP-*nudA*^{HC}; *gpdA*-ΔC-*hookA*-S-*AfpyrG*	This work
XX693	*kinA*^{K895*}; GFP-*nudA*^{R1602,K1645E}; *argB2::[argB*-alcAp*::mCherry-*RabA]*	This work
XX711	*kinA*($^{1-894)}$-GFP-*AfpyrG*; *alcA*-GFP-*myoV-pyr4*; *pyroA*4; *wA*2; possibly Δ*nkuA::argB*; possibly *pyrG*89	This work
XX713	*alcA*-GFP-*myoV-pyr4*; *pyroA*4; *wA*2; possibly Δ*nkuA::argB*; possibly *pyrG*89	This work
XX716	GFP-*nudA*^{HC}*;* Δ*hookA-AfpyrG; argB2::[argB*-alcAp*::mCherry-*RabA]*; w*A2*	This work
XX718	*kinA*^{K895*}; GFP-*nudA*^{HC}*;* Δ*hookA-AfpyrG; argB2::[argB*-alcAp*::mCherry-*RabA]*; w*A2*	This work
XX738	*kinA*^{K895*}; *argB2::[argB*-alcAp*::mCherry-*RabA]*; *pyrG*89; *wA2;* possibly Δ*nkuA::argB*	This work

XX752	*kinA*$^{(1\text{-}894)}$-GFP-*AfpyrG*; Δ*myoV*::*AfpyrG; pyrG*89; Δ*nkuA::argB; yA2*	This work
XX782	Δ*myoV*::*AfpyrG; argB*2*::[argB*-alcAp*::mCherry-*RabA];* possibly *pyrG*89; possibly Δ*nkuA::argB*	This work
XX810	diploid XX738/RQ197	This work
XX811	diploid RQ54/RQ197	This work
XX814	diploid RQ54/RQ358	This work
XX824	Δ*myoV*::*AfpyrG; rabE*p::GFP-RabE::*AfpyrG*::*rabE*; *argB*2*::[argB*-alcAp*::mCherry-*RabA]; pyrG*89; possibly Δ*nkuA::argB*	This work
XX825	*kinA*^{K895*}; Δ*myoV*::*AfpyrG; rabE*p::GFP-RabE::*AfpyrG*::*rabE*; *argB*2*::[argB*-alcAp*::mCherry-*RabA]; pyrG*89; possibly Δ*nkuA::argB*	This work
XX828	diploid XX738/RQ358	This work
XX834	*hookA*-GFP-*afpyrG*; *kinA*^{K895*}; *argB*2*::[argB*-alcAp*::mCherry-*RabA];* possibly *pyrG*89; possibly Δ*nkuA::argB*	This work
XX836	*nudA*^{R1602,K1645E}; *hookA*-GFP-*afpyrG*; *nudF*6; possibly *pyrG*89; possibly Δ*nkuA::argB*	This work
XX838	*hookA*-GFP-*afpyrG*; *nudF*6; possibly *pyrG*89; possibly Δ*nkuA::argB*	This work
XX842	*nudA*^{R1602,K1645E}; *hookA*-GFP-*afpyrG*; *kinA*^{K895*}; *argB*2*::[argB*-alcAp*::mCherry-*RabA];* possibly *pyrG*89; possibly Δ*nkuA::argB*	This work

Supplemental Figure 1. A sequence alignment of kinesin-1s including KIF5A, kinesin-1 heavy chain in Drosophila (Kin-1_Drosophil) and kinesin-1 in *Aspergillus nidulans* (KinA). The alignment was done using MacVector T-Coffee multiple sequence alignment (Pairwise Mode: Myers Miller). Residues that are identical (*), strongly similar (:) or weakly similar (.) are indicated. The IAK motif was highlighted in yellow and the C-terminal microtubule-binding domain was shaded with grey.

```
KIF5A              1 MAET---NNECSIKVLCRFRPLNQAEILRGDKFIPIFQGD---DSVVIGGK----PYVFD   50
Kin-1_Drosophil    1 MSAEREIPAEDSIKVVCRFRPLNDSEEKAGSKFVVKFPNNVEENCISIAGK----VYLFD   56
KinA               1 MASSTSN-PSNTIKVVARFRPQNKVELASGGQPIVEFEND---ETCSINSKEASGSFTFD   56
                     *.         .***..**** *  *   * . .  * .     .  *  *     . **

KIF5A             51 RVFPPNTTQEQVYHACAMQIVKDVLAGYNGTIFAYGQTSSGKTHTMEGK-LHDPQLMGII  109
Kin-1_Drosophil   57 KVFKPNASQEKVYNEAAKSIVTDVLAGYNGTIFAYGQTSSGKTHTMEGV-IGDSVKQGII  115
KinA              57 RVFPMDSKQTDVFNYSIAPTVDDILNGYNGTVFAYGQTGAGKSYTMMGSDIDDEVGKGII  116
                     .**   . *  *.. .    * *.* *****.****** .**. ** *  . *    ***

KIF5A            110 PRIARDIFNHIYSMDENLEFHIKVSYFEIYLDKIRDLLDVTKTNLSVHEDKNRVPFVKGC  169
Kin-1_Drosophil  116 PRIVNDIFNHIYAMEVNLEFHIKVSYYEIYMDKIRDLLDVSKVNLSVHEDKNRVPYVKGA  175
KinA             117 PRIVEQIFASILTSPSNIEYTVRVSYMEIYMERIRDLLVPQNDNLPVHEEKSRGVYVKGL  176
                     ***   **  * .   *.*. ..*** ***...*****     ** ***.* *  .***

KIF5A            170 TERFVSSPEEILDVIDEGKSNRHVAVTNMNEHSSRSHSIFLINIKQENMETEQKLSGKLY  229
Kin-1_Drosophil  176 TERFVSSPEDVFEVIEEGKSNRHIAVTNMNEHSSRSHSVFLINVKQENLENQKKLSGKLY  235
KinA             177 LEVYVSSVQEVYEVMRRGGNARAVAATNMNQESSRSHSIFVITVTQKNLETGSAKSGQLF  236
                      * .*** ... .*.  *   * .* ****. ******.*.*.. * *.*.    **.*.

KIF5A            230 LVDLAGSEKVSKTGAEGAVLDEAKNINKSLSALGNVISALAEGTKSYVPYRDSKMTRILQ  289
Kin-1_Drosophil  236 LVDLAGSEKVSKTGAEGTVLDEAKNINKSLSALGNVISALADGNKTHIPYRDSKLTRILQ  295
KinA             237 LVDLAGSEKVGKTGASGQTLEEAKKINKSLSALGMVINALTDGKSTHIPYRDSKLTRILQ  296
                     ********** **** *  *.*** ********* ** **..*  . .******.*****

KIF5A            290 DSLGGNCRTTMFICCSPSSYNDAETKSTLMFGQRAKTIKNTASVNLELTAEQWKKKYEKE  349
Kin-1_Drosophil  296 ESLGGNARTTIVICCSPASFNESETKSTLDFGRRAKTVKNVVCVNEELTAEEWKRRYEKE  355
KinA             297 ESLGGNSRTTLIINCSPSSYNDAETVSTLRFGVRAKAIKNKAKVNAELSPAELKQLLRRA  356
                     .*****.***. * ***.*.*..** *** ** ***..**   ** **.  . *.   .

KIF5A            350 KEKTKAQKETIAKLEAELSRWRNGENVPETERLAGEE-----------AALGAELCE---  395
Kin-1_Drosophil  356 KEKNARLKGKVEKLEIELARWRAGETVKAEEQINMEDLMEASTPNLEVEAAQTAAAEAA-  414
KinA             357 QSQVTSFENYISALESEVSSWRSGETVPREKWT----------PARNAEAVGAAKAEARG  406
                     . .       .  ** *.. ** **.*                    *  .  .*

KIF5A            396 ----E-TPVNDNSSIVVRIAPEERQKYE-------------------EEIRRLYKQLDDK  431
Kin-1_Drosophil  415 -LAAQRTALAN-MS--ASVAVNEQARLA-------------------TECERLYQQLDDK  451
KinA             407 PRPSTPSRLHD-VS--RSETPRPDSRIGDRSSTPSIVLEKDEREEFLRRENELQDQIAEK  463
                           . .    *     .     .                        *  *. .*

KIF5A            432 DDEINQQSQLIEKLKQQMLDQEELLVSTRGDNEKVQRELSHLQSENDAAKDEVKEVLQAL  491
Kin-1_Drosophil  452 DEEINQQSQYAEQLKEQVMEQEELIANARREYETLQSEMARIQQENESAKEEVKEVLQAL  511
KinA             464 ESHIATIERGLR--------------EARDELRTLKENSARSGKDNEKLNAEVNELRMHL  509
                     .  *    .                 .* .   ..   ..   .*.    ** *.   *

KIF5A            492 EELAVNYDQKSQEVEEKSQQNQLLVDELSQ-KVATMLSLESELQRLQEVSGHQRKRIAEV  550
Kin-1_Drosophil  512 EELAVNYDQKSQEIDNKNKDIDALNEELQQ-KQSVFNAASTELQQLKDMSSHQKKRITEM  570
KinA             510 EKVSYESKEAAITMDSLREANSELTAELDEVKQQLLDVRMKAKETTAALDEKEKKK-AEK  568
                     * ..    . .  ..        *  ** . *          .    .  ...*. .*

KIF5A            551 LNGLMKDLSEFSVIVGNGEIKLPVEIS-------GAIEEEFTVARLYISKIKSEVKSVVK  603
Kin-1_Drosophil  571 LTNLLRDLGEVGQAIAPGESSIDLKMSALAGTDASKVEEDFTMARLFISKMKTEAKNIAQ  630
KinA             569 MA--------------------------------KMMAGFDLGGEVFSDNERKLQNLIQ  595
                     .                                 .   * .     *      . . .
KIF5A            604 RCRQLENLQVECH-----RKMEVTGRELSSCQLLISQHEAKIRSLTEYMQSVELKKRHLE  658
Kin-1_Drosophil  631 RCSNMETQQADSN-----KKISEYEKDLGEYRLLISQHEARMKSLQESMREAENKKRTLE  685
KinA             596 RVDSLHQ-IAEAGEVIAPDDLLELRASLSETQGFIRQAELTVNDRSELNVLQDSRRMELE  654
                     *   .     ..        .      *   .  * * *  .    *     . ..  **
```

```
KIF5A            659 ESYDSLSDELAKLQAQETVHEVALKDKEPDTQDADEVKKALELQMESHREAHHRQLARLR  718
Kin-1_Drosophil  686 EQIDSLREECAKLKAAEHVSAVNAEEK----QRAEELRSMFDSQMDELREAHTRQVSELR  741
KinA             655 QKLANLEQDYESLLARNLGEEDLAEIK----ERLEKV-------YIAKKDVELAAASELQ  703
                     .    *  .   * *           *    .  . .           ..      . *.

KIF5A            719 DEINEKQKTIDELKDLNQKLQLELEKLQADYEKLKSEEHEKSTKLQELTFLYERHEQSKQ  778
Kin-1_Drosophil  742 DEIAAKQHEMDEMKDVHQKLLLAHQQMTADYEKVRQEDAEKSSELQNIILTNERREQARK  801
KinA             704 QQLARKDEELTK-----------LQQSLADS-------------------------QSRG  727
                      ..  *   .              ..  **                          *..

KIF5A            779 DLKGL-EETVARELQTLHNLRKLFVQDVTTRVKKSAEME-PED-----------SGGIHS  825
Kin-1_Drosophil  802 DLKGL-EDTVAKELQTLHNLRKLFVQDLQQRIRKNVVNEESEE-----------DGGSLA  849
KinA             728 STNGAASKSLQQQIAEFDAMKKSLMRDLQNRCERVVELEISLDDAREQYNNVLRSSNNRA  787
                        *    .. ...     ..*  ..*.  *  .    *   .            .  .

KIF5A            826 QKQKISFLENNLEQLTKVHKQLVRDNADLRCELPKLEKRLRATAERVKALEGALKEAKEG  885
Kin-1_Drosophil  850 QKQKISFLENNLDQLTKVHKQLVRDNADLRCELPKLEKRLRCTMERVKALETALKEAKEG  909
KinA             788 QQKKMAFLERNLEQLTHVQRQLVEQNSSLKKEVAIAERKLIARNERISSLEALLQESQEK  847
                     *..*..*** **.***.*..***  *. *. *.   *..* .  **. .**  *.*..*

KIF5A            886 AMKDKRRYQQEVDRIKEAVRYKSSGK-------------RGHSAQIAKPVRPGHYPASSP  932
Kin-1_Drosophil  910 AMRDRKRYQYEVDRIKEAVRQKHLGR-------------RGPQAQIAKPIRSGQGA----  952
KinA             848 LTQANHRFEAQLTAVKERLEAAKQGSTKGLPGMDSNGGFSFAGSRIAKPLRGGG------  901
                       .  .*.. ..  .** .     *                  ..***.* *

KIF5A            933 TNPYGTRSPECISYTNSLFQNYQNLYLQATPSSTSDMYFANSCTSSGATSSGGPLASYQK  992
Kin-1_Drosophil  953 ----------------------------------------IAIRGGGAVGGPSPLAQVNP  972
KinA             902 --------------------------------------------------GGNEPVAAVQS  912
                                                                          *.*  .

KIF5A            993 ANMDNGNATDINDNRSDLPCGYEAEDQAKLFPLHQETAAS 1032
Kin-1_Drosophil  973 VN-------------------------------------S  975
KinA             913 QDTGTKRTSWFFDR------------------------R  927
```

Supplemental Figure 2. The *kinA*^{k895*} or the *kinA*$^{(1-894)}$-GFP allele causes a defect in dynein-mediated early endosome transport in diploids with the presence of full-length *kinA*. (A) Microscopic images showing the distributions of mCherry-RabA-labeled early endosomes in four different diploids. Hyphal tip is indicated by a yellow arrowhead. Bar, 5 μm. (B) A quantitative analysis on the percentage of hyphal tips with the abnormal accumulation of early endosomes. Three experiments were performed, and in each experiment, 30 or more hyphal tips were examined for each strain. Scatter plots with mean and S.D. values were generated by Prism 9. ****p<0.0001; *p<0.05; ns, non-significant or p>0.05 (Ordinary one-way ANOVA, unpaired).

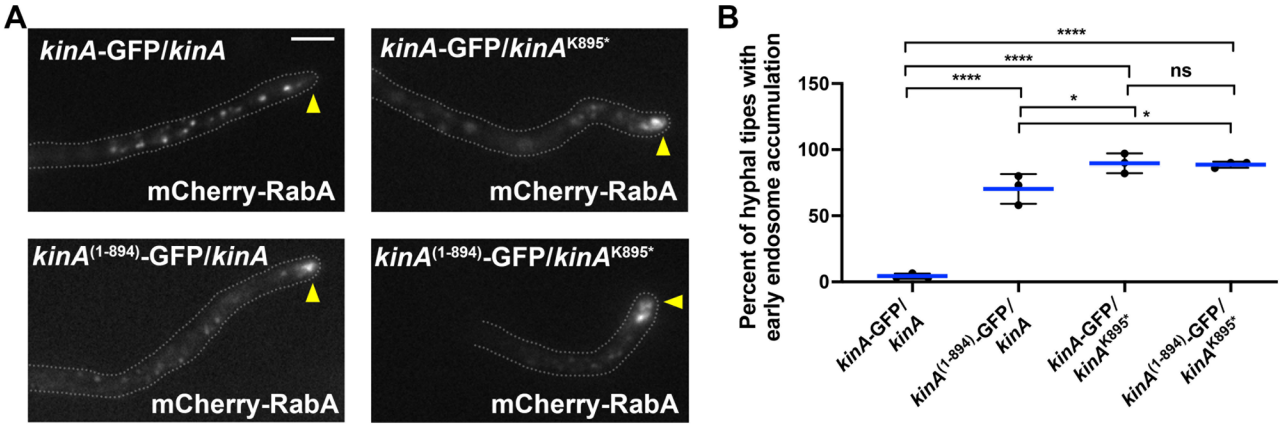

References

Abenza, J.F., A. Pantazopoulou, J.M. Rodriguez, A. Galindo, and M.A. Penalva. 2009. Long-distance movement of Aspergillus nidulans early endosomes on microtubule tracks. *Traffic*. 10:57-75.

Ally, S., A.G. Larson, K. Barlan, S.E. Rice, and V.I. Gelfand. 2009. Opposite-polarity motors activate one another to trigger cargo transport in live cells. *J Cell Biol*. 187:1071-1082.

Arimoto, M., S.P. Koushika, B.C. Choudhary, C. Li, K. Matsumoto, and N. Hisamoto. 2011. The Caenorhabditis elegans JIP3 protein UNC-16 functions as an adaptor to link kinesin-1 with cytoplasmic dynein. *J Neurosci*. 31:2216-2224.

Baron, D.M., A.R. Fenton, S. Saez-Atienzar, A. Giampetruzzi, A. Sreeram, Shankaracharya, P.J. Keagle, V.R. Doocy, N.J. Smith, E.W. Danielson, M. Andresano, M.C. McCormack, J. Garcia, V. Bercier, L. Van Den Bosch, J.R. Brent, C. Fallini, B.J. Traynor, E.L.F. Holzbaur, and J.E. Landers. 2022. ALS-associated KIF5A mutations abolish autoinhibition resulting in a toxic gain of function. *Cell Rep*. 39:110598.

Baumbach, J., A. Murthy, M.A. McClintock, C.I. Dix, R. Zalyte, H.T. Hoang, and S.L. Bullock. 2017. Lissencephaly-1 is a context-dependent regulator of the human dynein complex. *Elife*. 6.

Bielska, E., M. Schuster, Y. Roger, A. Berepiki, D.M. Soanes, N.J. Talbot, and G. Steinberg. 2014. Hook is an adapter that coordinates kinesin-3 and dynein cargo attachment on early endosomes. *J Cell Biol*. 204:989-1007.

Blasius, T.L., D. Cai, G.T. Jih, C.P. Toret, and K.J. Verhey. 2007. Two binding partners cooperate to activate the molecular motor Kinesin-1. *J Cell Biol*. 176:11-17.

Boecker, C.A., J. Goldsmith, D. Dou, G.G. Cajka, and E.L.F. Holzbaur. 2021. Increased LRRK2 kinase activity alters neuronal autophagy by disrupting the axonal transport of autophagosomes. *Curr Biol*. 31:2140-2154 e2146.

Brendza, R.P., L.R. Serbus, W.M. Saxton, and J.B. Duffy. 2002. Posterior localization of dynein and dorsal-ventral axis formation depend on kinesin in Drosophila oocytes. *Curr Biol*. 12:1541-1545.

Byrd, D.T., M. Kawasaki, M. Walcoff, N. Hisamoto, K. Matsumoto, and Y. Jin. 2001. UNC-16, a JNK-signaling scaffold protein, regulates vesicle transport in C. elegans. *Neuron*. 32:787-800.

Cai, D., A.D. Hoppe, J.A. Swanson, and K.J. Verhey. 2007. Kinesin-1 structural organization and conformational changes revealed by FRET stoichiometry in live cells. *J Cell Biol*. 176:51-63.

Canty, J.T., A. Hensley, A. Yildiz. 2021. TRAK adaptors coordinate the recruitment and activation of dynein and kinesin to control mitochondrial transport. bioRxiv doi: https://doi.org/10.1101/2021.07.30.454553

Carvalho, P., M.L. Gupta, Jr., M.A. Hoyt, and D. Pellman. 2004. Cell cycle control of kinesin-mediated transport of Bik1 (CLIP-170) regulates microtubule stability and dynein activation. *Dev Cell*. 6:815-829.

Celestino, R., J.B. Gama, A.F. Castro-Rodrigues, D.J. Barbosa, E.A. d'Amico, A. Musacchio, A.X. Carvalho, J.H. Morais-Cabral, R. Gassmann. 2021. JIP3 regulates bi-directional organelle transport in neurons through its interaction with dynein and kinesin-1. bioRxiv doi: https://doi.org/10.1101/2021.10.11.463801

Chen, Y., and Z.H. Sheng. 2013. Kinesin-1-syntaphilin coupling mediates activity-dependent regulation of axonal mitochondrial transport. *J Cell Biol*. 202:351-364.

Chevalier-Larsen, E., and E.L. Holzbaur. 2006. Axonal transport and neurodegenerative disease. *Biochim Biophys Acta*. 1762:1094-1108.

Christensen, J.R., A.A. Kendrick, J.B. Truong, A. Aguilar-Maldonado, V. Adani, M. Dzieciatkowska, and S.L. Reck-Peterson. 2021. Cytoplasmic dynein-1 cargo diversity is mediated by the combinatorial assembly of FTS-Hook-FHIP complexes. *Elife*. 10.

Cox, R.T., and A.C. Spradling. 2006. Milton controls the early acquisition of mitochondria by Drosophila oocytes. *Development*. 133:3371-3377.

Coy, D.L., W.O. Hancock, M. Wagenbach, and J. Howard. 1999. Kinesin's tail domain is an inhibitory regulator of the motor domain. *Nat Cell Biol*. 1:288-292.

Duncan, J.E., and R. Warrior. 2002. The cytoplasmic dynein and kinesin motors have interdependent roles in patterning the Drosophila oocyte. *Curr Biol*. 12:1982-1991.

Efimov, V.P., J. Zhang, and X. Xiang. 2006. CLIP-170 homologue and NUDE play overlapping roles in NUDF localization in Aspergillus nidulans. *Mol Biol Cell*. 17:2021-2034.

Egan, M.J., K. Tan, and S.L. Reck-Peterson. 2012. Lis1 is an initiation factor for dynein-driven organelle transport. *J Cell Biol*. 197:971-982.

Elshenawy, M.M., E. Kusakci, S. Volz, J. Baumbach, S.L. Bullock, and A. Yildiz. 2020. Lis1 activates dynein motility by modulating its pairing with dynactin. *Nat Cell Biol*.

Fenton, A.R., T.A. Jongens, and E.L.F. Holzbaur. 2021. Mitochondrial adaptor TRAK2 activates and functionally links opposing kinesin and dynein motors. *Nat Commun*. 12:4578.

Ferro, L.S., Q. Fang, L. Eshun-Wilson, J. Fernandes, A. Jack, D.P. Farrell, M. Golcuk, T. Huijben, K. Costa, M. Gur, F. DiMaio, E. Nogales, and A. Yildiz. 2022. Structural and functional insight into regulation of kinesin-1 by microtubule-associated protein MAP7. *Science*. 375:326-331.

Fu, M.M., and E.L. Holzbaur. 2013. JIP1 regulates the directionality of APP axonal transport by coordinating kinesin and dynein motors. *J Cell Biol*. 202:495-508.

Fu, M.M., and E.L. Holzbaur. 2014. Integrated regulation of motor-driven organelle transport by scaffolding proteins. *Trends Cell Biol*. 24:564-574.

Gao, X., M. Schmid, Y. Zhang, S. Fukuda, N. Takeshita, and R. Fischer. 2019. The spindle pole body of Aspergillus nidulans is asymmetrical and contains changing numbers of gamma-tubulin complexes. *J Cell Sci*. 132.

Gennerich, A., and R.D. Vale. 2009. Walking the walk: how kinesin and dynein coordinate their steps. *Curr Opin Cell Biol*. 21:59-67.

Gershoni-Emek, N., A. Mazza, M. Chein, T. Gradus-Pery, X. Xiang, K.W. Li, R. Sharan, and E. Perlson. 2016. Proteomic Analysis of Dynein-Interacting Proteins in Amyotrophic Lateral

Sclerosis Synaptosomes Reveals Alterations in the RNA-Binding Protein Staufen1. *Mol Cell Proteomics*. 15:506-522.

Gillies, J.P., J.M. Reimer, E.P. Karasmanis, I. Lahiri, Z.M. Htet, A.E. Leschziner, and S.L. Reck-Peterson. 2022. Structural basis for cytoplasmic dynein-1 regulation by Lis1. *Elife*. 11.

Gindhart, J.G., Jr., C.J. Desai, S. Beushausen, K. Zinn, and L.S. Goldstein. 1998. Kinesin light chains are essential for axonal transport in Drosophila. *J Cell Biol*. 141:443-454.

Guardia, C.M., A. Jain, R. Mattera, A. Friefeld, Y. Li, and J.S. Bonifacino. 2021. RUSC2 and WDR47 oppositely regulate kinesin-1-dependent distribution of ATG9A to the cell periphery. *Mol Biol Cell*. 32:ar25.

Guo, X., G.G. Farias, R. Mattera, and J.S. Bonifacino. 2016. Rab5 and its effector FHF contribute to neuronal polarity through dynein-dependent retrieval of somatodendritic proteins from the axon. *Proc Natl Acad Sci U S A*. 113:E5318-5327.

Hafezparast, M., R. Klocke, C. Ruhrberg, A. Marquardt, A. Ahmad-Annuar, S. Bowen, G. Lalli, A.S. Witherden, H. Hummerich, S. Nicholson, P.J. Morgan, R. Oozageer, J.V. Priestley, S. Averill, V.R. King, S. Ball, J. Peters, T. Toda, A. Yamamoto, Y. Hiraoka, M. Augustin, D. Korthaus, S. Wattler, P. Wabnitz, C. Dickneite, S. Lampel, F. Boehme, G. Peraus, A. Popp, M. Rudelius, J. Schlegel, H. Fuchs, M. Hrabe de Angelis, G. Schiavo, D.T. Shima, A.P. Russ, G. Stumm, J.E. Martin, and E.M. Fisher. 2003. Mutations in dynein link motor neuron degeneration to defects in retrograde transport. *Science*. 300:808-812.

Han, G., B. Liu, J. Zhang, W. Zuo, N.R. Morris, and X. Xiang. 2001. The Aspergillus cytoplasmic dynein heavy chain and NUDF localize to microtubule ends and affect microtubule dynamics. *Curr Biol*. 11:719-724.

Hirokawa, N., R. Sato-Yoshitake, T. Yoshida, and T. Kawashima. 1990. Brain dynein (MAP1C) localizes on both anterogradely and retrogradely transported membranous organelles in vivo. *J Cell Biol*. 111:1027-1037.

Hirokawa, N., and Y. Tanaka. 2015. Kinesin superfamily proteins (KIFs): Various functions and their relevance for important phenomena in life and diseases. *Exp Cell Res*. 334:16-25.

Htet, Z.M., J.P. Gillies, R.W. Baker, A.E. Leschziner, M.E. DeSantis, and S.L. Reck-Peterson. 2020. LIS1 promotes the formation of activated cytoplasmic dynein-1 complexes. *Nat Cell Biol*.

Ikenaka, K., K. Kawai, M. Katsuno, Z. Huang, Y.M. Jiang, Y. Iguchi, K. Kobayashi, T. Kimata, M. Waza, F. Tanaka, I. Mori, and G. Sobue. 2013. dnc-1/dynactin 1 knockdown disrupts transport of autophagosomes and induces motor neuron degeneration. *PLoS One*. 8:e54511.

Januschke, J., L. Gervais, S. Dass, J.A. Kaltschmidt, H. Lopez-Schier, D. St Johnston, A.H. Brand, S. Roth, and A. Guichet. 2002. Polar transport in the Drosophila oocyte requires Dynein and Kinesin I cooperation. *Curr Biol*. 12:1971-1981.

Jha, R., J. Roostalu, N.I. Cade, M. Trokter, and T. Surrey. 2017. Combinatorial regulation of the balance between dynein microtubule end accumulation and initiation of directed motility. *Embo j*. 36:3387-3404.

Kaan, H.Y., D.D. Hackney, and F. Kozielski. 2011. The structure of the kinesin-1 motor-tail complex reveals the mechanism of autoinhibition. *Science*. 333:883-885.

Kelliher, M.T., Y. Yue, A. Ng, D. Kamiyama, B. Huang, K.J. Verhey, and J. Wildonger. 2018. Autoinhibition of kinesin-1 is essential to the dendrite-specific localization of Golgi outposts. *J Cell Biol*. 217:2531-2547.

Keren-Kaplan, T., and J.S. Bonifacino. 2021. ARL8 Relieves SKIP Autoinhibition to Enable Coupling of Lysosomes to Kinesin-1. *Curr Biol*. 31:540-554.e545.

Kieran, D., M. Hafezparast, S. Bohnert, J.R. Dick, J. Martin, G. Schiavo, E.M. Fisher, and L. Greensmith. 2005. A mutation in dynein rescues axonal transport defects and extends the life span of ALS mice. *J Cell Biol*. 169:561-567.

Konzack, S., P.E. Rischitor, C. Enke, and R. Fischer. 2005. The role of the kinesin motor KipA in microtubule organization and polarized growth of Aspergillus nidulans. *Mol Biol Cell*. 16:497-506.

Kruppa, A.J., and F. Buss. 2021. Motor proteins at the mitochondria-cytoskeleton interface. *J Cell Sci*. 134.

Lammers, L.G., and S.M. Markus. 2015. The dynein cortical anchor Num1 activates dynein motility by relieving Pac1/LIS1-mediated inhibition. *J Cell Biol*. 211:309-322.

LaMonte, B.H., K.E. Wallace, B.A. Holloway, S.S. Shelly, J. Ascaño, M. Tokito, T. Van Winkle, D.S. Howland, and E.L. Holzbaur. 2002. Disruption of dynein/dynactin inhibits axonal transport in motor neurons causing late-onset progressive degeneration. *Neuron*. 34:715-727.

Lau, C.K., F.J. O'Reilly, B. Santhanam, S.E. Lacey, J. Rappsilber, and A.P. Carter. 2021. Cryo-EM reveals the complex architecture of dynactin's shoulder region and pointed end. *Embo j*. 40:e106164.

Lenz, J.H., I. Schuchardt, A. Straube, and G. Steinberg. 2006. A dynein loading zone for retrograde endosome motility at microtubule plus-ends. *Embo j*. 25:2275-2286.

Lloyd, T.E., J. Machamer, K. O'Hara, J.H. Kim, S.E. Collins, M.Y. Wong, B. Sahin, W. Imlach, Y. Yang, E.S. Levitan, B.D. McCabe, and A.L. Kolodkin. 2012. The p150(Glued) CAP-Gly domain regulates initiation of retrograde transport at synaptic termini. *Neuron*. 74:344-360.

Lu, W., M. Winding, M. Lakonishok, J. Wildonger, and V.I. Gelfand. 2016. Microtubule-microtubule sliding by kinesin-1 is essential for normal cytoplasmic streaming in Drosophila oocytes. *Proc Natl Acad Sci U S A*. 113:E4995-5004.

Maimon, R., L. Ankol, T. Gradus Pery, T. Altman, A. Ionescu, R. Weissova, M. Ostrovsky, E. Tank, G. Alexandra, N. Shelestovich, Y. Opatowsky, A. Dori, S. Barmada, M. Balastik, and E. Perlson. 2021. A CRMP4-dependent retrograde axon-to-soma death signal in amyotrophic lateral sclerosis. *Embo j*. 40:e107586.

Markus, S.M., and W.L. Lee. 2011. Regulated offloading of cytoplasmic dynein from microtubule plus ends to the cortex. *Dev Cell*. 20:639-651.

Marzo, M.G., J.M. Griswold, and S.M. Markus. 2020. Pac1/LIS1 stabilizes an uninhibited conformation of dynein to coordinate its localization and activity. *Nat Cell Biol*.

McKenney, R.J., W. Huynh, M.E. Tanenbaum, G. Bhabha, and R.D. Vale. 2014. Activation of cytoplasmic dynein motility by dynactin-cargo adapter complexes. *Science*. 345:337-341.

Mentis, A.A., D. Vlachakis, E. Papakonstantinou, I. Zaganas, G.P. Patrinos, G.P. Chrousos, and E. Dardiotis. 2022. A novel

variant in DYNC1H1 could contribute to human amyotrophic lateral sclerosis-frontotemporal dementia spectrum. *Cold Spring Harb Mol Case Stud*. 8.

Monroy, B.Y., T.C. Tan, J.M. Oclaman, J.S. Han, S. Simó, S. Niwa, D.W. Nowakowski, R.J. McKenney, and K.M. Ori-McKenney. 2020. A Combinatorial MAP Code Dictates Polarized Microtubule Transport. *Dev Cell*. 53:60-72.e64.

Moughamian, A.J., and E.L. Holzbaur. 2012. Dynactin is required for transport initiation from the distal axon. *Neuron*. 74:331-343.

Münch, C., R. Sedlmeier, T. Meyer, V. Homberg, A.D. Sperfeld, A. Kurt, J. Prudlo, G. Peraus, C.O. Hanemann, G. Stumm, and A.C. Ludolph. 2004. Point mutations of the p150 subunit of dynactin (DCTN1) gene in ALS. *Neurology*. 63:724-726.

Nakano, J., K. Chiba, and S. Niwa. 2022. An ALS-associated KIF5A mutant forms oligomers and aggregates and induces neuronal toxicity. *Genes Cells*.

Nayak, T., E. Szewczyk, C.E. Oakley, A. Osmani, L. Ukil, S.L. Murray, M.J. Hynes, S.A. Osmani, and B.R. Oakley. 2006. A versatile and efficient gene-targeting system for Aspergillus nidulans. *Genetics*. 172:1557-1566.

Nicolas, A., K.P. Kenna, A.E. Renton, N. Ticozzi, F. Faghri, R. Chia, J.A. Dominov, B.J. Kenna, M.A. Nalls, P. Keagle, A.M. Rivera, W. van Rheenen, N.A. Murphy, J. van Vugt, J.T. Geiger, R.A. Van der Spek, H.A. Pliner, Shankaracharya, B.N. Smith, G. Marangi, S.D. Topp, Y. Abramzon, A.S. Gkazi, J.D. Eicher, A. Kenna, G. Mora, A. Calvo, L. Mazzini, N. Riva, J. Mandrioli, C. Caponnetto, S. Battistini, P. Volanti, V. La Bella, F.L. Conforti, G. Borghero, S. Messina, I.L. Simone, F. Trojsi, F. Salvi, F.O. Logullo, S. D'Alfonso, L. Corrado, M. Capasso, L. Ferrucci, C.A.M. Moreno, S. Kamalakaran, D.B. Goldstein, A.D. Gitler, T. Harris, R.M. Myers, H. Phatnani, R.L. Musunuri, U.S. Evani, A. Abhyankar, M.C. Zody, J. Kaye, S. Finkbeiner, S.K. Wyman, A. LeNail, L. Lima, E. Fraenkel, C.N. Svendsen, L.M. Thompson, J.E. Van Eyk, J.D. Berry, T.M. Miller, S.J. Kolb, M. Cudkowicz, E. Baxi, M. Benatar, J.P. Taylor, E. Rampersaud, G. Wu, J. Wuu, G. Lauria, F. Verde, I. Fogh, C. Tiloca, G.P. Comi, G. Sorarù, C. Cereda, P. Corcia, H. Laaksovirta, L. Myllykangas, L. Jansson, M. Valori, J. Ealing, H. Hamdalla, S. Rollinson, S. Pickering-Brown, R.W. Orrell, K.C. Sidle, A. Malaspina, J. Hardy, A.B. Singleton, J.O. Johnson, S. Arepalli, P.C. Sapp, D. McKenna-Yasek, et al. 2018. Genome-wide Analyses Identify KIF5A as a Novel ALS Gene. *Neuron*. 97:1268-1283.e1266.

Oakley, B.R., C.E. Oakley, Y. Yoon, and M.K. Jung. 1990. Gamma-tubulin is a component of the spindle pole body that is essential for microtubule function in Aspergillus nidulans. *Cell*. 61:1289-1301.

Olenick, M.A., R. Dominguez, and E.L.F. Holzbaur. 2019. Dynein activator Hook1 is required for trafficking of BDNF-signaling endosomes in neurons. *J Cell Biol*. 218:220-233.

Pant, D.C., J. Parameswaran, L. Rao, L. Shi, G. Chilukuri, Z.T. McEachin, J. Glass, G.J. Bassell, A. Gennerich, J. Jiang. 2022. ALS-linked KIF5A ΔExon27 mutant causes neuronal toxicity through gain of function. bioRxiv: doi https://doi.org/10.1101/2022.03.05.483071

Pantazopoulou, A., M. Pinar, X. Xiang, and M.A. Peñalva. 2014. Maturation of late Golgi cisternae into RabE(RAB11) exocytic post-Golgi carriers visualized in vivo. *Mol Biol Cell*. 25:2428-2443.

Penalva, M.A., J. Zhang, X. Xiang, and A. Pantazopoulou. 2017. Transport of fungal RAB11 secretory vesicles involves myosin-5, dynein/dynactin/p25, and kinesin-1 and is independent of kinesin-3. *Mol Biol Cell*. 28:947-961.

Pinar, M., and M.A. Peñalva. 2021. The fungal RABOME: RAB GTPases acting in the endocytic and exocytic pathways of Aspergillus nidulans (with excursions to other filamentous fungi). *Mol Microbiol*. 116:53-70.

Pinar, M., A. Alonso, V. de los Ríos, I. Bravo-Plaza, Á. Gandara, E. Arias-Palomo, M.Á. Peñalva. 2021. A novel RAB11-containing adaptor complex anchoring myosin-5 to secretory vesicles.bioRxiv: doi https://doi.org/10.1101/2021.09.12.459962

Qiu, R., J. Zhang, J.D. Rotty, and X. Xiang. 2021. Dynein activation in vivo is regulated by the nucleotide states of its AAA3 domain. *Curr Biol*. 31:4486-4498.e4486.

Qiu, R., J. Zhang, and X. Xiang. 2013. Identification of a novel site in the tail of dynein heavy chain important for dynein function in vivo. *J Biol Chem*. 288:2271-2280.

Qiu, R., J. Zhang, and X. Xiang. 2018. p25 of the dynactin complex plays a dual role in cargo binding and dynactin regulation. *J Biol Chem*. 293:15606-15619.

Qiu, R., J. Zhang, and X. Xiang. 2019. LIS1 regulates cargo-adapter-mediated activation of dynein by overcoming its autoinhibition in vivo. *J Cell Biol*. 218:3630-3646.

Qiu, R., J. Zhang, and X. Xiang. 2020. The splicing-factor Prp40 affects dynein-dynactin function in Aspergillus nidulans. *Mol Biol Cell*:mbcE20030166.

Requena, N., C. Alberti-Segui, E. Winzenburg, C. Horn, M. Schliwa, P. Philippsen, R. Liese, and R. Fischer. 2001. Genetic evidence for a microtubule-destabilizing effect of conventional kinesin and analysis of its consequences for the control of nuclear distribution in Aspergillus nidulans. *Mol Microbiol*. 42:121-132.

Roberts, A.J., B.S. Goodman, and S.L. Reck-Peterson. 2014. Reconstitution of dynein transport to the microtubule plus end by kinesin. *Elife*. 3:e02641.

Roney, J.C., S. Li, T. Farfel-Becker, N. Huang, T. Sun, Y. Xie, X.T. Cheng, M.Y. Lin, F.M. Platt, and Z.H. Sheng. 2021. Lipid-mediated motor-adaptor sequestration impairs axonal lysosome delivery leading to autophagic stress and dystrophy in Niemann-Pick type C. *Dev Cell*. 56:1452-1468.e1458.

Sakamoto, R., D.T. Byrd, H.M. Brown, N. Hisamoto, K. Matsumoto, and Y. Jin. 2005. The Caenorhabditis elegans UNC-14 RUN domain protein binds to the kinesin-1 and UNC-16 complex and regulates synaptic vesicle localization. *Mol Biol Cell*. 16:483-496.

Salogiannis, J., and S.L. Reck-Peterson. 2017. Hitchhiking: A Non-Canonical Mode of Microtubule-Based Transport. *Trends Cell Biol*. 27:141-150.

Schlager, M.A., H.T. Hoang, L. Urnavicius, S.L. Bullock, and A.P. Carter. 2014. In vitro reconstitution of a highly processive recombinant human dynein complex. *EMBO J*. 33:1855-1868.

Schuchardt, I., D. Assmann, E. Thines, C. Schuberth, and G. Steinberg. 2005. Myosin-V, Kinesin-1, and Kinesin-3 cooperate in hyphal growth of the fungus Ustilago maydis. *Mol Biol Cell*. 16:5191-5201.

Schuster, M., S. Treitschke, S. Kilaru, J. Molloy, N.J. Harmer, and G. Steinberg. 2012. Myosin-5, kinesin-1 and myosin-17

cooperate in secretion of fungal chitin synthase. *Embo j*. 31:214-227.

Seiler, S., J. Kirchner, C. Horn, A. Kallipolitou, G. Woehlke, and M. Schliwa. 2000. Cargo binding and regulatory sites in the tail of fungal conventional kinesin. *Nat Cell Biol*. 2:333-338.

Splinter, D., D.S. Razafsky, M.A. Schlager, A. Serra-Marques, I. Grigoriev, J. Demmers, N. Keijzer, K. Jiang, I. Poser, A.A. Hyman, C.C. Hoogenraad, S.J. King, and A. Akhmanova. 2012. BICD2, dynactin, and LIS1 cooperate in regulating dynein recruitment to cellular structures. *Mol Biol Cell*. 23:4226-4241.

Stavoe, A.K.H., and E.L.F. Holzbaur. 2019. Axonal autophagy: Mini-review for autophagy in the CNS. *Neurosci Lett*. 697:17-23.

Ström, A.L., J. Gal, P. Shi, E.J. Kasarskis, L.J. Hayward, and H. Zhu. 2008. Retrograde axonal transport and motor neuron disease. *J Neurochem*. 106:495-505.

Szewczyk, E., T. Nayak, C.E. Oakley, H. Edgerton, Y. Xiong, N. Taheri-Talesh, S.A. Osmani, and B.R. Oakley. 2006. Fusion PCR and gene targeting in Aspergillus nidulans. *Nat Protoc*. 1:3111-3120.

Taheri-Talesh, N., Y. Xiong, and B.R. Oakley. 2012. The functions of myosin II and myosin V homologs in tip growth and septation in Aspergillus nidulans. *PLoS One*. 7:e31218.

Torisawa, T., M. Ichikawa, A. Furuta, K. Saito, K. Oiwa, H. Kojima, Y.Y. Toyoshima, and K. Furuta. 2014. Autoinhibition and cooperative activation mechanisms of cytoplasmic dynein. *Nat Cell Biol*. 16:1118-1124.

Twelvetrees, A.E., F. Lesept, E.L.F. Holzbaur, and J.T. Kittler. 2019. The adaptor proteins HAP1a and GRIP1 collaborate to activate the kinesin-1 isoform KIF5C. *J Cell Sci*. 132.

Twelvetrees, A.E., S. Pernigo, A. Sanger, P. Guedes-Dias, G. Schiavo, R.A. Steiner, M.P. Dodding, and E.L. Holzbaur. 2016. The Dynamic Localization of Cytoplasmic Dynein in Neurons Is Driven by Kinesin-1. *Neuron*. 90:1000-1015.

Vaughan, P.S., P. Miura, M. Henderson, B. Byrne, and K.T. Vaughan. 2002. A role for regulated binding of p150(Glued) to microtubule plus ends in organelle transport. *J Cell Biol*. 158:305-319.

Verhey, K.J., and J.W. Hammond. 2009. Traffic control: regulation of kinesin motors. *Nat Rev Mol Cell Biol*. 10:765-777.

Wedlich-Soldner, R., A. Straube, M.W. Friedrich, and G. Steinberg. 2002. A balance of KIF1A-like kinesin and dynein organizes early endosomes in the fungus Ustilago maydis. *EMBO J*. 21:2946-2957.

Williams, L.S., S. Ganguly, P. Loiseau, B.F. Ng, and I.M. Palacios. 2014. The auto-inhibitory domain and ATP-independent microtubule-binding region of Kinesin heavy chain are major functional domains for transport in the Drosophila germline. *Development*. 141:176-186.

Willins, D.A., X. Xiang, and N.R. Morris. 1995. An alpha tubulin mutation suppresses nuclear migration mutations in Aspergillus nidulans. *Genetics*. 141:1287-1298.

Winding, M., M.T. Kelliher, W. Lu, J. Wildonger, and V.I. Gelfand. 2016. Role of kinesin-1-based microtubule sliding in Drosophila nervous system development. *Proc Natl Acad Sci U S A*. 113:E4985-4994.

Wong, Y.L., K.A. Dietrich, N. Naber, R. Cooke, and S.E. Rice. 2009. The Kinesin-1 tail conformationally restricts the nucleotide pocket. *Biophys J*. 96:2799-2807.

Xiang, X., G. Han, D.A. Winkelmann, W. Zuo, and N.R. Morris. 2000. Dynamics of cytoplasmic dynein in living cells and the effect of a mutation in the dynactin complex actin-related protein Arp1. *Curr Biol*. 10:603-606.

Xiang, X., and R. Qiu. 2020. Cargo-Mediated Activation of Cytoplasmic Dynein in vivo. *Front Cell Dev Biol*. 8:598952.

Xiang, X., W. Zuo, V.P. Efimov, and N.R. Morris. 1999. Isolation of a new set of Aspergillus nidulans mutants defective in nuclear migration. *Curr Genet*. 35:626-630.

Xiong, Y., and B.R. Oakley. 2009. In vivo analysis of the functions of gamma-tubulin-complex proteins. *J Cell Sci*. 122:4218-4227.

Xu, J., B.J. Reddy, P. Anand, Z. Shu, S. Cermelli, M.K. Mattson, S.K. Tripathy, M.T. Hoss, N.S. James, S.J. King, L. Huang, L. Bardwell, and S.P. Gross. 2012. Casein kinase 2 reverses tail-independent inactivation of kinesin-1. *Nat Commun*. 3:754.

Yamada, M., S. Toba, T. Takitoh, Y. Yoshida, D. Mori, T. Nakamura, A.H. Iwane, T. Yanagida, H. Imai, L.Y. Yu-Lee, T. Schroer, A. Wynshaw-Boris, and S. Hirotsune. 2010. mNUDC is required for plus-end-directed transport of cytoplasmic dynein and dynactins by kinesin-1. *EMBO J*. 29:517-531.

Yang, L., L. Ukil, A. Osmani, F. Nahm, J. Davies, C.P. De Souza, X. Dou, A. Perez-Balaguer, and S.A. Osmani. 2004. Rapid production of gene replacement constructs and generation of a green fluorescent protein-tagged centromeric marker in Aspergillus nidulans. *Eukaryot Cell*. 3:1359-1362.

Yao, X., X. Wang, and X. Xiang. 2014. FHIP and FTS proteins are critical for dynein-mediated transport of early endosomes in Aspergillus. *Mol Biol Cell*. 25:2181-2189.

Yao, X., J. Zhang, H. Zhou, E. Wang, and X. Xiang. 2012. In vivo roles of the basic domain of dynactin p150 in microtubule plus-end tracking and dynein function. *Traffic*. 13:375-387.

Yeh, T.Y., N.J. Quintyne, B.R. Scipioni, D.M. Eckley, and T.A. Schroer. 2012. Dynactin's pointed-end complex is a cargo-targeting module. *Mol Biol Cell*. 23:3827-3837.

Zekert, N., and R. Fischer. 2009. The Aspergillus nidulans kinesin-3 UncA motor moves vesicles along a subpopulation of microtubules. *Mol Biol Cell*. 20:673-684.

Zeng, C.J., H.R. Kim, I. Vargas Arispuro, J.M. Kim, A.C. Huang, and B. Liu. 2014. Microtubule plus end-tracking proteins play critical roles in directional growth of hyphae by regulating the dynamics of cytoplasmic microtubules in Aspergillus nidulans. *Mol Microbiol*. 94:506-521.

Zhang, J., S. Li, R. Fischer, and X. Xiang. 2003. Accumulation of cytoplasmic dynein and dynactin at microtubule plus ends in Aspergillus nidulans is kinesin dependent. *Mol Biol Cell*. 14:1479-1488.

Zhang, J., R. Qiu, H.N. Arst, Jr., M.A. Penalva, and X. Xiang. 2014. HookA is a novel dynein-early endosome linker critical for cargo movement in vivo. *J Cell Biol*. 204:1009-1026.

Zhang, J., K. Tan, X. Wu, G. Chen, J. Sun, S.L. Reck-Peterson, J.A. Hammer, 3rd, and X. Xiang. 2011a. Aspergillus myosin-V supports polarized growth in the absence of microtubule-based transport. *PLoS One*. 6:e28575.

Zhang, J., X. Yao, L. Fischer, J.F. Abenza, M.A. Penalva, and X. Xiang. 2011b. The p25 subunit of the dynactin complex is required for dynein-early endosome interaction. *J Cell Biol*. 193:1245-1255.

Zhang, J., L. Zhuang, Y. Lee, J.F. Abenza, M.A. Penalva, and X. Xiang. 2010. The microtubule plus-end localization of Aspergillus dynein is important for dynein-early-endosome interaction but not for dynein ATPase activation. *J Cell Sci*. 123:3596-3604.

Zhang, K., H.E. Foster, A. Rondelet, S.E. Lacey, N. Bahi-Buisson, A.W. Bird, and A.P. Carter. 2017a. Cryo-EM Reveals How Human Cytoplasmic Dynein Is Auto-inhibited and Activated. *Cell*. 169:1303-1314.e1318.

Zhang, Y., X. Gao, R. Manck, M. Schmid, A.H. Osmani, S.A. Osmani, N. Takeshita, and R. Fischer. 2017b. Microtubule-organizing centers of Aspergillus nidulans are anchored at septa by a disordered protein. *Mol Microbiol*. 106:285-303.

Zhao, Y., E. Song, W. Wang, C.H. Hsieh, X. Wang, W. Feng, X. Wang, and K. Shen. 2021. Metaxins are core components of mitochondrial transport adaptor complexes. *Nat Commun*. 12:83.

Zhuang, L., J. Zhang, and X. Xiang. 2007. Point mutations in the stem region and the fourth AAA domain of cytoplasmic dynein heavy chain partially suppress the phenotype of NUDF/LIS1 loss in Aspergillus nidulans. *Genetics*. 175:1185-1196.